DYN-1 regulates SPD-2 and PLK-1 localization and mitotic spindle pole organization

Carter Dierlam[1], Stephanie Held[2], Jiya Hastings[2], Livinus Anyanwu[3], Robert H. Newman[2], and Jyoti Iyer[2]*

[1]Department of Cell Biology and Molecular Genetics, University of Maryland College Park, College Park, MD 20742, [2]Department of Biology, North Carolina Agricultural and Technical State University, Greensboro, NC 27411, and [3]Department of Chemistry and Biochemistry, University of Tulsa, Tulsa, OK 74104.

Number of characters = 19,997

Running title: *DYN-1 regulates SPD-2 and PLK-1*

*To whom correspondence should be addressed:

Jyoti Iyer

Email: jgiyer@ncat.edu; Tel. (336) 285-4573

Keywords: dynamin, PLK-1, SPD-2, mitosis, midbody, centrosome

ABSTRACT

Accurate mitosis is essential for genome stability. Although dynamin is best known for its role in vesicular trafficking, its functions during mitosis remain unclear. Here, we identify a mitotic role for the *C. elegans* dynamin homolog DYN-1 in regulating spindle assembly and the localization of the key mitotic regulators SPD-2 and PLK-1. Depletion of DYN-1 results in enlarged metaphase spindle poles and increased centrosomal SPD-2 and PLK-1 levels. These effects likely depend on DYN-1-mediated vesicular trafficking, as shown by assays with the *dyn-1(ky51)* allele. Additionally, a subset of DYN-1-depleted embryos exhibit altered PLK-1 localization at the midbody during late mitosis, correlating with midbody assembly defects. Together, these findings establish DYN-1 as a previously unrecognized regulator of spindle pole organization and early midbody assembly.

SIGNIFICANCE STATEMENT

Dynamin is primarily known for its function in endocytosis, but its involvement in mitosis is not well defined. This study shows that dynamin helps organize mitotic spindle poles, ensures proper centrosome localization of SPD-2 and PLK-1, and supports early steps of midbody assembly in *C. elegans* embryos. These findings reveal a previously unrecognized mitotic role for dynamin and suggest new links between membrane dynamics, spindle organization, and the cytokinetic machinery.

39 **INTRODUCTION**

40 Accurate cell division is essential for proper chromosome segregation, and mitotic errors
41 can lead to aneuploidy—a distinguishing feature of many cancers (Levine and Holland, 2018).
42 Understanding the molecular mechanisms that regulate mitosis is therefore critical. The GTPase
43 dynamin is a large ~100 kDa protein that is best known for its role in the scission of endocytic
44 vesicles (Hinshaw, 2000; Praefcke and McMahon, 2004). *C. elegans* possesses a single classical
45 dynamin encoded by the *dyn-1* gene (Clark *et al*., 1997). Interestingly, some of the earliest
46 studies identified dynamin as a microtubule-binding protein (Paschal *et al.*, 1987; Shpetner and
47 Vallee, 1989). However, dynamin's function in microtubule-associated processes such as spindle
48 assembly and midbody organization during mitosis is not well understood. While DYN-1 was
49 shown to localize to the midbody (Thompson *et al.*, 2002), and mediate membrane remodeling
50 during the late stages of abscission (König *et al.*, 2017), its potential role in early midbody
51 assembly remains unexplored.

52 The coiled-coil protein SPindle Defective 2 (SPD-2) (the *C. elegans* homolog of human
53 CEP192) is essential for proper centrosome biogenesis and spindle assembly during mitosis
54 (O'Connell *et al.*, 2000; Kemp *et al.*, 2004; Pelletier *et al.*, 2004; Gomez-Ferreria *et al.*, 2007,
55 Zhu *et al.*, 2008). SPD-2 levels at the centrosomes are regulated by proteins including SAS-7,
56 SPD-5, DHC-1 and AIR-1, among others (Sugioka *et al.*, 2017; Kemp *et al.*, 2004; Pelletier *et*
57 *al.*, 2004). Proper levels of centrosome-associated SPD-2 are required for proper centriole
58 duplication, pericentriolar material (PCM) organization and spindle assembly (O'Connell *et al.*,
59 2000; Kemp *et al.*, 2004; Pelletier *et al.*, 2004). SPD-2 directly binds to the kinase Polo-like
60 kinase 1 (PLK-1) to recruit the kinase to the centrosomes (Boxem *et al.,* 2008; Decker *et al.,*
61 2011).

62 PLK1 is a mitotic master regulator that is essential for several mitotic processes including
63 mitotic entry, centrosome dynamics, chromosome congression, chromosome alignment and
64 cytokinesis (Petronczki *et al.,* 2008; Archambault and Glover, 2009; Zitouni *et al.,* 2014). PLK1
65 exhibits a dynamic localization pattern at different stages of mitosis. During early mitosis, PLK1
66 localizes prominently to the centrosomes, and the kinetochores. At anaphase, it re-localizes to the
67 spindle midzone and at telophase, it becomes enriched at the midbody (Golsteyn *et al.,* 1995; Lee
68 *et al.,* 1995; Arnaud *et al.,* 1998; Barr *et al.*, 2004; Petronczki *et al.,* 2008; Schmucker and
69 Sumara, 2014). The timely localization of PLK1 to various cellular components is essential for
70 its different important roles during mitosis. Importantly, removal of PLK1 from the centrosomes
71 is required for proper mitotic progression (Kishi *et al.,* 2009). Although the kinase activity of
72 PLK1 is thought to be required for PLK1 removal from the centrosomes (Kishi *et al.,* 2009), the
73 mechanism by which PLK1 is removed from the centrosomes remains unclear.

74 **RESULTS AND DISCUSSION**

75 ***dyn-1* depletion results in abnormal metaphase spindle pole assembly and increased levels**
76 **of SPD-2**

77 To determine the effect of DYN-1 depletion in *C. elegans* embryos, we knocked down
78 endogenous DYN-1 using *RNAi* (Supplemental Figure S1, A and B). Interestingly, DYN-1–
79 depleted embryos (n=20) were noticeably smaller than controls (n=23), exhibiting a reduced
80 average cytoplasmic area (~906 μm^2 vs. ~1200 μm^2; $p < 0.0001$) (Supplemental Figure S1, C
81 and D). DYN-1 was previously shown to localize to the mitotic spindle at metaphase, suggesting
82 a potential role in metaphase spindle assembly (Thompson *et al.,* 2002). To determine the effect
83 of DYN-1 depletion on metaphase spindle assembly, we examined the effect of DYN-1 depletion
84 on spindle pole size using mCherry::tubulin as a proxy (Figure 1). Upon measuring spindle pole

85 area, we determined that DYN-1-depleted embryos (n=58 spindle poles) exhibited larger spindle
86 poles than control (*smd-1(RNAi)*)-depleted embryos (n=53 spindle poles; p=0.0018) (Figure 1, A
87 and B). Specifically, the mean spindle pole area of control RNAi embryos was 14.6 μm^2 while
88 that of *dyn-1(RNAi)* embryos was 17.36 μm^2. Thus, our data have identified a novel role for the
89 endocytic protein DYN-1 in regulating metaphase spindle pole assembly. An important regulator
90 of spindle pole and centrosome size is the PCM protein SPD-2 (O'Connell *et al.*, 2000; Kemp *et*
91 *al.*, 2004; Pelletier *et al.*; Decker *et al.,* 2011). Therefore, we asked whether SPD-2 levels at the
92 centrosomes were altered between control RNAi and *dyn-1(RNAi)* treated embryos. Our analysis
93 indicated that centrosome-associated SPD-2 levels were significantly increased ~1.7-fold upon
94 DYN-1 depletion (Figure 1, C and D; n=66 for *dyn-1(RNAi)*; n=60 for controls; $p < 0.0001$).

95 **DYN-1 depletion increases levels of centrosome-associated PLK-1**

96 Because SPD-2 directly binds to PLK-1 and recruits it to centrosomes (Boxem *et al.,* 2008;
97 Decker *et al.,* 2011), and SPD-2 levels increase upon DYN-1 depletion (Figure 1, C and D), we
98 next asked whether PLK-1 also becomes elevated at centrosomes under these conditions. To
99 determine if DYN-1 depletion affects centrosomal PLK-1, we performed live imaging on a strain
100 co-expressing mCherry::tubulin and CRISPR-tagged endogenous PLK-1::sfGFP (Martino *et al.,*
101 2017). We then knocked down endogenous DYN-1 in this strain using *RNAi* and performed live
102 imaging of control (*smd-1*(*RNAi)*) and *dyn-1(RNAi)* treated embryos using spinning-disk
103 confocal microscopy. Consistent with our hypothesis, our analysis revealed that PLK-1 levels at
104 the centrosomes were significantly elevated upon DYN-1 depletion (Figure 2, A and B).
105 Specifically, we found that PLK-1 intensity was ~2.5-fold higher in *dyn-1(RNAi)* embryos
106 (n=52) than controls (n=58; $p < 0.0001$) (Figure 2, A and B).

107 The *dyn-1(ky51)* GTPase mutant, which perturbs vesicular trafficking (Clark *et al.*, 1997;
108 Grant and Hirsch, 1999), also exhibited increased centrosomal PLK-1 (Figure 2). Specifically,
109 PLK-1 levels were on average elevated ~1.85-fold at *dyn-1(ky51)* centrosomes (n=46
110 centrosomes) as compared with control centrosomes (n=44 centrosomes; $p<0.0001$) (Figure 2, C
111 and D). These data indicate that the vesicular trafficking function of DYN-1 is required for its
112 regulation of centrosome-associated PLK-1 levels. Furthermore, these data also confirm the
113 specificity of our *dyn-1(RNAi)* phenotype.
114 Endogenous PLK-1 is a low-abundance protein in wild-type (N2) whole-worm lysates
115 (Chen *et al.*, 2023), and the preparation of embryonic extracts is technically labor-intensive.
116 Therefore, to sensitively assess whether total PLK-1 levels differ between control and *dyn-*
117 *1(ky51)* embryos, we measured PLK-1::sfGFP fluorescence intensity in the anterior and posterior
118 cytoplasm of metaphase embryos (Supplemental Figure S2). We reasoned that if total PLK-1
119 levels are increased upon impairing DYN-1 function, we should see a proportional increase in
120 cytoplasmic PLK-1 fluorescence in the *dyn-1(ky51)* embryos. Our analysis revealed a modest
121 ~7% increase in PLK-1 levels in the anterior and posterior cytoplasm of *dyn-1(ky51)* embryos as
122 compared with controls ($p=0.0234$ (anterior), $p=0.0318$ (posterior)) (Supplemental Figure S2).
123 Given that PLK-1 levels at metaphase centrosomes increase by ~1.85-fold in *dyn-1(ky51)*
124 embryos (Figure 2, C and D), this modest ~1.07-fold increase in cytoplasmic PLK-1 is unlikely
125 to fully explain the elevated centrosome-associated PLK-1 levels observed in these mutants.

126 **PLK-1 persists at the centrosomes following DYN-1 depletion in a subset of embryos**
127 **during the later stages of mitosis**

128 PLK-1 exhibits a spatially and temporally regulated localization pattern during different stages of
129 mitosis (Chase *et al.,* 2000; Budirahardja and Gönczy, 2008; Martino *et al.,* 2017). It transitions

130 from its location at the centrosomes and the kinetochores during early mitosis, to the spindle
131 midzone and the midbody during late mitosis (Chase *et al.,* 2000; Budirahardja and Gönczy,
132 2008; Martino *et al.,* 2017). While performing live imaging, we noticed several embryos where
133 PLK-1 appeared to persist at the centrosomes (specifically at the PCM) during the later stages of
134 mitosis (Figure 3A). To quantify this phenotype, we analyzed PLK-1::sfGFP fluorescence
135 intensity at anterior centrosomes at different cell cycle stages in both control RNAi and *dyn-*
136 *1(RNAi)* treated embryos (Figure 3; Supplemental Figure S3). Note that we measured PLK-
137 1::sfGFP at anterior centrosomes only because cytoplasmic background is more uniform there; in
138 contrast, the posterior cytoplasm contains punctate, uneven PLK-1 that makes measurements
139 unreliable. Our quantitative analysis revealed that there was no PLK-1 detectable at any of the
140 control centrosomes analyzed at 39±4 seconds post early telophase (n=29 centrosomes) (Figure
141 3, A and B; Supplemental Figure S3). In contrast, in 35% of the centrosomes from *dyn-1(RNAi)*
142 treated embryos (9 out of 26 centrosomes), PLK-1 was still detectable at the centrosomes at this
143 stage (p=0.0005) (Figure 3, A and B; Supplemental Figure S3).
144 We also noted a statistically significant increase in centrosome-associated PLK-1::sfGFP
145 upon *dyn-1(RNAi)* (n=26 centrosomes) as compared with controls (n=29 centrosomes) via an
146 unpaired two-tailed t-test at early anaphase (p<0.0001), late anaphase (p=0.0004) as well as in
147 early telophase (p=0.0094) (Supplemental Figure S3). These data indicate that a pool of PLK-1
148 tends to persist at the centrosomes of DYN-1-depleted embryos during the later stages of mitosis.
149 **DYN-1-depleted embryos exhibit abnormal midbody formation**
150 Since DYN-1 has a known role in cytokinesis and localizes to the midbody (Thompson *et al.,*
151 2002), we analyzed midbody formation in DYN-1-depleted embryos. Intercellular bridge (IB)
152 assembly, assessed using mCherry::tubulin fluorescence, served as a proxy for midbody

153 formation (Hu *et al.*, 2012; Green *et al.,* 2013; König *et al.*, 2017). We noted that all of the
154 control RNAi embryos (n=19 embryos) exhibited a normal tubulin-intense IB during telophase
155 (Figure 4, A (white arrows) and B). In contrast, 50% of the *dyn-1(RNAi)* embryos (12 out of 24
156 embryos) did not exhibit any detectable IB during telophase (Figure 4, A (bottom panel) and B).
157 Interestingly, 50% of the *dyn-1(RNAi)* embryos exhibited a structurally abnormal IB that either
158 started forming outside the reference time-window for normal IB assembly (normal IB started
159 forming between 195 to 390 seconds post-metaphase) or exhibited defects in IB assembly
160 dynamics (Figure 4, A (middle panel) and B). Importantly, the *dyn-1(ky51)* allele also exhibited
161 mild defects in IB assembly (Figure 4B), demonstrating the specificity of this phenotype. While
162 previous ultrastructural analysis identified a role for DYN-1 in membrane remodeling during the
163 late stages of abscission (König et al., 2017), our study identifies a novel requirement for DYN-1
164 in regulating midbody organization during the initial stages of this process. Together, these data
165 suggest that DYN-1 function is required for proper midbody assembly.

166 **PLK-1 localization to the midbody is defective in DYN-1-depleted embryos**

167 Given that PLK-1 persists at the centrosomes through late mitosis in a subset of DYN-1-depleted
168 embryos (Figure 3), we hypothesized that this retention might correlate with abnormal PLK-1
169 dynamics at the midbody. To investigate this, we analyzed PLK-1 localization using two
170 complementary approaches: a time-matched analysis and an event-matched analysis. The time-
171 matched analysis (Figure 5, A and B) examined whether PLK-1 localized to midbodies that
172 started forming during the standard developmental window for IB assembly (195–390 seconds
173 post-metaphase). Conversely, the event-matched analysis evaluated PLK-1 recruitment
174 specifically when an IB eventually formed, regardless of timing.

175 Our time-matched analysis revealed that PLK-1 failed to localize to the midbody in 83%
176 of *dyn-1(RNAi)* embryos (n = 24), compared to 100% localization in controls (n = 19; $p <$
177 0.0001; Figure 5A). To distinguish whether this reduction was simply due to a failure in
178 midbody formation, we performed an event-matched analysis restricted to *dyn-1(RNAi)* embryos
179 where an IB-like structure was present (n = 12). Importantly, PLK-1 localized to these formed
180 midbodies to varying degrees in all cases: 42% showed relatively normal accumulation, while
181 58% exhibited fragmented, weak, or near-background signals (Figure 5, A and C; p=0.0003).
182 Together, these data demonstrate that even when a midbody successfully forms following *dyn-1*
183 depletion, PLK-1 recruitment is frequently altered rather than entirely absent. Notably, due to
184 inconsistent background signals resulting from polarity defects in *dyn-1(RNAi)* embryos, we
185 were unable to reliably quantify PLK-1::sfGFP fluorescence intensity at midbodies, as these
186 background fluorescence fluctuations often led to inconsistent measurements.
187 In summary, our studies have identified a new role for the endocytic protein DYN-1 in
188 regulating metaphase spindle assembly, early midbody assembly and the localization of the
189 mitotic proteins SPD-2 and PLK-1. Specifically, we find that upon DYN-1 depletion, SPD-2 and
190 PLK-1 accumulate at the centrosomes in metaphase and this is associated with aberrant
191 metaphase spindle pole assembly. Furthermore, while PLK-1 is normally removed from the
192 centrosomes during late mitosis, upon DYN-1 depletion, we find that PLK-1 persists at a subset
193 of centrosomes during the later stages of mitosis.
194 Based upon our data, we propose a model whereby DYN-1 regulates the levels of SPD-2
195 and PLK-1 at metaphase centrosomes, potentially through a vesicular trafficking mechanism.
196 DYN-1 depletion leads to elevated SPD-2 levels at metaphase centrosomes, and because SPD-2
197 is a known upstream recruiter of PLK-1 (Boxem *et al.*, 2008; Decker *et al.*, 2011), this increase

198 in SPD-2 is accompanied by increased PLK-1 accumulation at centrosomes. The elevated levels
199 of these PCM components are associated with aberrant spindle pole assembly. In late mitosis,
200 DYN-1 depletion also disrupts the normal relationship between midbody formation and PLK-1
201 accumulation at the IB: embryos frequently fail to assemble a midbody, and even in cases where
202 a midbody-like structure does form, PLK-1 enrichment is often fragmented or reduced. While we
203 cannot yet distinguish whether altered PLK-1 midbody localization reflects defective midbody
204 assembly, impaired PLK-1 recruitment, or a combination of both, our findings indicate that
205 DYN-1 is required for coordinating the proper redistribution of PLK-1 between centrosomes and
206 the midbody.

207 The defects in midbody assembly were more pronounced in *dyn-1(RNAi)* embryos than in
208 *dyn-1(ky51)* mutants. Correspondingly, PLK-1::sfGFP enrichment at metaphase centrosomes
209 was higher following *dyn-1(RNAi)* (~2.5-fold) compared to *dyn-1(ky51)* (~1.85-fold). These
210 observations suggest that *dyn-1(ky51)* may be a hypomorphic allele. Alternatively, DYN-1 may
211 regulate these processes through mechanisms other than its role in vesicular trafficking. Future
212 studies should investigate these potential roles, including whether DYN-1 physically interacts
213 with PLK-1 to facilitate its recruitment or turnover. Rescue approaches using hypomorphic *plk-1*
214 alleles may also help clarify the contribution of PLK-1 dysregulation to causality of the observed
215 defects, but such experiments are beyond the scope of the present work. It will also be important
216 to determine whether the DYN-1→SPD-2→PLK-1 pathway is conserved in other organisms.

217 Since our studies also uncovered the regulation of centrosome-associated SPD-2 levels
218 by DYN-1, an important next step is to determine the specific mechanism of this regulation.
219 Since SPD-2 is an upstream component of the PCM assembly pathway (Kemp *et al.*, 2004),
220 future studies will examine whether centrosome levels of other PCM proteins, such as PCMD-1,

221 SAS-7, SPD-5, and AIR-1, are also altered upon DYN-1 depletion. Investigating these broader
222 effects will clarify whether the role of DYN-1 is specific to the SPD-2/PLK-1 axis or if it
223 influences centrosome composition and mitotic spindle assembly more generally.

224 **MATERIALS AND METHODS**

225 ***C. elegans* strains growth and maintenance**

226 All *C. elegans* strains described in this study were grown and maintained using standard
227 techniques on OP50 seeded Modified Youngren's Only Bacto-peptone (MYOB) agar plates at
228 20ºC (the strains were shifted to other assay-specific temperatures as needed).

229 ***C. elegans* strains and genetic crosses**

230 The wild-type N2 strain and the OD2425 strain expressing PLK-1::sfGFP (*plk-1(lt18[plk-*
231 *1::sfGFP]::loxp) III)* (Martino *et al.,* 2017) were obtained from the *Caenorhabditis Genetics*
232 *Center* (CGC). The OC908 strain (*bsSi30[pCW9: unc-119(+) pcdk-11.2::sfgfp::his-58::cdk-11.2*
233 *3' UTR] II; bsIs20[pNP99: unc-119(+) tbb-1p::mCherry::tbb-2::tbb-2 3'-UTR]; bsIs2[pCK5.5:*
234 *Ppie-1::gfp::spd-2]*) and the OC779 strain (*bsSi15[pKO109: spd-2p-spd-2::mCherry::spd-2 3'-*
235 *utr, unc-119(+)] I; bsSi30[pCW9: unc-119(+) pcdk-11.2::sfgfp::his-58::cdk-11.2 3' utr] II; unc-*
236 *119(ed3) III*) were obtained from Dr. Kevin O'Connell's laboratory at NIDDK, NIH. The
237 mCherry::tubulin–expressing strain IYR028 (*bsIs20[pNP99: unc-119(+) tbb-1p::mCherry::tbb-*
238 *2::tbb-2 3'-UTR]*) was generated in our laboratory by crossing OC908 hermaphrodites with N2
239 males and isolating progeny expressing only mCherry::tubulin. Following this, mCherry::tubulin
240 expressing males were generated from the IYR028 strain by heat shock at 30°C for 6 hours.
241 These mCherry::tubulin males from the IYR028 strain were then crossed with PLK-1::sfGFP
242 expressing hermaphrodites from the OD2425 strain to generate the IYR038 strain
243 (*bsIs20[pNP99: unc-119(+) tbb-1p::mCherry::tbb-2::tbb-2 3'-UTR]; plk-1(lt18[plk-*

244 *1::sGFP]::loxP) III)* which was homozygous for both mCherry::tubulin and PLK-1::sfGFP. This
245 strain was validated for homozygosity of the two loci by confocal microscopy. The IYR035
246 strain (*dyn-1(luv35[ky51]) X*) was generated by CRISPR/Cas9 editing as described previously
247 (Paix *et al.,* 2015; Paix *et al.,* 2016; Iyer *et al.,* 2018; Smith *et al.*, 2020). This strain was
248 confirmed by both PCR and restriction digestion with Pst1 followed by agarose gel
249 electrophoresis as well as by DNA sequencing. The IYR043 strain (*bsIs20[pNP99: unc-119(+)*
250 *tbb-1p::mCherry::tbb-2::tbb-2 3'-UTR]; plk-1(lt18[plk-1::sfGFP]::loxP) III; dyn-*
251 *1(luv35[ky51]) X*) was homozygous for the *dyn-1(ky51)* mutation, mCherry::tubulin and PLK-
252 1::sfGFP. The IYR044 strain (*bsIs20[pNP99: unc-119(+) tbb-1p::mCherry::tbb-2::tbb-2 3'-*
253 *UTR]; plk-1(lt18[plk-1::sfGFP]::loxP) III; dyn-1(+) X*) was homozygous for mCherry::tubulin,
254 PLK-1::sfGFP and wild-type for *dyn-1*. The IYR043 and IYR044 strains were both generated by
255 crossing IYR035 hermaphrodites with IYR038 males (the males were made by heat shock at
256 30°C for 6 hours). Both these strains were validated by confocal microscopy for homozygosity of
257 the fluorescent markers (mCherry::tubulin and PLK-1::sfGFP). PCR and Pst1 digestion followed
258 by agarose gel electrophoresis as well as by DNA sequencing was used to confirm homozygosity
259 of the *dyn-1(ky51)* mutation (IYR043) and wild-type *dyn-1* (IYR044).

260 **CRISPR/Cas9 editing**

261 CRISPR/Cas9 genome editing utilizing assembled ribonucleoprotein complexes and a linear
262 DNA repair template (Paix *et al.,* 2015; Paix *et al.,* 2016) was performed to generate the IYR035
263 strain (*dyn-1(luv35[ky51]) X*) according to the protocols detailed in Iyer *et al.* (2018) and Smith
264 *et al.* (2020). The sequences of the editing reagents used to create this strain are as follows:
265 *dyn-1(ky51)* crRNA: 5'- TGAATAAGCTGCAAAATAAG -3'

266 *dyn-1(ky51)* repair template (silent mutations introduce a Pst1 restriction site): 5'-
267 AGACTTCTTGCCACGTGGATCAGGAATCGTAACACGTCGTTCATTGATCCTGCAGCT
268 TATTCAAGATCGCAATGAGTACGCCGAGTTCCTAC -3'
269 *dyn-1(ky51)* screening primers:
270 *dyn-1(ky51)* forward: 5'- CGTTGATCCCTGTGATCAAT – 3'
271 *dyn-1(ky51)* reverse: 5'- TTTCAGATGCTCAAATCATCC – 3'
272 ***RNAi* by feeding**
273 HT115 bacteria expressing the *dyn-1(RNAi)* construct were purchased from Horizon Discovery
274 Ltd. (Lafayette, CO) while HT115 bacteria expressing the *smd-1 RNAi* construct (control) were
275 obtained from Dr. Kevin O'Connell's laboratory (NIDDK, Bethesda, MD). HT115 *E. coli*
276 transformed with either control (*smd-1(RNAi)*) or *dyn-1(RNAi)* plasmids were grown on MYOB
277 plates supplemented with 100 µg/ml carbenicillin and 2 mM Isopropyl β- d-1-
278 thiogalactopyranoside (IPTG) as described previously (Kamath and Ahringer J 2003; Iyer *et al.,*
279 2022). Briefly, L4-stage *C. elegans* from the IYR038 strain were transferred onto *RNAi* plates
280 and incubated at 25 ºC for 24 to 36 hours. Gravid adults from these plates were then dissected to
281 release their embryos and 1-cell stage embryos were analyzed by confocal live imaging.
282 **Conditions for wild-type and *dyn-1(ky51)* worms**
283 Starved plates with the IYR043 (*dyn-1(ky51)*) and IYR044 (wild-type *dyn-1*) strains were
284 washed with M9 buffer and used to seed large 10 cm MYOB plates. These plates were placed at
285 26 ºC until L4s appeared. 100 to 125 L4s were picked from each plate and transferred onto new
286 individual 10 cm MYOB plates at 26 ºC overnight. Embryos from both strains were imaged the
287 next day using a spinning-disk confocal microscope.
288 **Sequence of *dyn-1(RNAi)* construct**

289 The commercially purchased *dyn-1(RNAi)* construct (Horizon Discovery Inc.) was subjected to
290 whole plasmid sequencing (Plasmidsaurus). The targeting sequence was found to be as follows:
291 5'-
292 ATGTCGTGGCAAAACCAGGGAATGCAGGCGTTGATCCCTGTGATCAATCGTGTCCAG
293 GACGCCTTCTCCCAGCTGGGCACATCTGTCAGCTTCGAACTTCCACAGATCGCCGTC
294 GTCGGAGGACAGTCCGCTGGAAAGTCGTCGGTGCTGGAGAATTTTGTCGGAAAAGA
295 CTTCTTGCCACGTGGATCAGGAATCGTAACACGTCGTCCACTTATTTTGCAGCTTATT
296 CAAGATCGCAATGAGTACGCCGAGTTCCTACACAAGAAGGGTCATCGCTTTGTGGAT
297 TTTGATGCAGTTCGGAAAGAGATTGAGGATGAGACTGATCGTGTCACTGGACAGAA
298 TAAGGGAATCAGTCCACATCCAATCAACTTGCGTGTCTTTTCTCCAAATGTTCTAAAT
299 CTGACACTCATCGATTTGCCCGGTCTCACAAAAGTGCCCGTCGGAGATCAACCAGCA
300 GATATTGAGCAACAGATCCGTGACATGATTCTCACATTCATCAACCGTGAGACTTGC
301 CTCATTCTTGCCGTCACTCCGGCCAACAGCGATCTCGCCACTTCGGATGCGTTGAAA
302 CTTGCGAAGGAAGTCGATCCACAGGGTCTTCGCACGATTGGAGCCCTCACCAAACTT
303 GACTTGATGGACGAGGGAACCGATGCTCGCGAGATCCTCGAGAACAAGCTGTTCAC
304 ACTTCGTCGTGGCTACGTCGGAGTTGTCAATCGTGGGCAGAAGGATATTGTCGGTCG
305 CAAGGATATTAGAGCTGCTTTGGACGCCGAGAGAAAGTTCTTCATCTCACACCCATC
306 CTACCGACATATGGCTGATCGGTTGGGAACAAGCTACCTTCAACACACTCTTAATCA
307 ACAGCTCACCAATCATATCCGTGATACACTGCCAACACTTCGTGATAGTCTTCAAAA
308 GAAGATGTTTGCTATGGAAAAGGATGTGGCCGAGTACAAGAACTACCAGCCAAATG
309 ATCCAGGCCGCAAGACCAAGGCTCTTTTGCAAATGGTTACCCAGTTCAATGCTGACA
310 TTGAGCGCTCCATTGAAGGTTCCTCTGCAAAGCTGGTTTCAGCCAATGAGCTCAGTG
311 GAGGAGCCCGTATCAATCGGCTTTTCCATGAGCGTTTCCCATTTGAGATTGTTAAAA

312 TGGAAATTGACGAGAAAGAAATGCGCAAAGAAATCCAGTATGCCATCAGAAACATT

313 CACGGTATCCGCGTCGGTCTCTTCACTCCGGATATGGCGTTTGAGGCAATTGCCAAA

314 AAGCAAATCACCCGTCTGAAGGAGCCATCGTTGAAATGCGTTGATCTGGTGGTCAAC

315 GAGTTGGCTAATGTGATCAGACAGTGCGCTGACACTATGGCTAGATATCCACGTCTT

316 CGTGACGAGCTGGAAAGAATCGTCGTCTCGCATATGCGTGAACGTGAGCAAATTGC

317 CAAGCAGCAAATTGGGCTCATTGTTGACTACGAACTCGCTTATATGAACACAAACCA

318 TGAGGATTTCATTGGATTCAGCAATGCTGAAGCAAAAGCCTCCCAAGGACAATCAG

319 CGAAGAAGAATCTTGGAAACCAGGTGATCAGAAAGGGCTGGCTCTCACTGAGCAAC

320 GTATCGTTTGTGCGTGGCTCCAAGGACAATTGGTTTGTGCTCATGTCGGACAGTTTG

321 AGTTGGTACAAAGATGATGAGGAGAAGGAGAAGAAGTACATGCTCCCATTGGATGG

322 TGTCAAGCTGAAGGATATTGAGGGTGGATTTATGTCTCGTAACCACAAGTTTGCTCT

323 GTTCTACCCCGACGGAAAGAACATCTACAAGGATTACAAGCAGCTTGAGTTGGGAT

324 GCACCAATTTGGACGAAATTGATGCGTGGAAGGCTTCATTCTTGCGTGCTGGTGTCT

325 ATCCAGAAAAGCAGAAGGCACAGGAAGATGAGTCCCAACAAGAGATGGAGGATAC

326 CTCGATTGATCCACAACTTGAGAGACAGGTGGAGACAATCCGTAATTTGGTTGATTC

327 CTACATGAGAATCATTACCAAGACAATTAAGGACCTGGTTCCAAAGGCGGTGATGC

328 ATTTGATTGTTAACCAGACAGGTGAGTTCATGAAAGATGAACTTTTGGCCCATCTCT

329 ACCAATGCGGCGACACTGATGCTCTCATGGAGGAATCTCAAATAGAAGCCCAGAAG

330 CGCGAGGAGATGCTCCGAATGTACCATGCTTGCAAGGAGGCGCTCCGCATTATCTCT

331 GAAGTCAACATGAGCACCCTTGGCGACCAGCCGCCGCCATTGCCGATGTCTGACTAC

332 CGCCCACACCCATCTGGACCTTCACCGGTGCCGCGTCCGGCTCCTGCTCCACCAGGC

333 GGACGTCAGGCCCCAATGCCACCACGCGGAGGACCCGGTGCCCCACCACCACCAGG

334 CATGAGACCACCACCAGGTGCGCCAGGAGGCGGCGGTGGCATGTACCCACCGTTGA
335 TTCCAAC- 3'

336 ***dyn-1* RT-PCR**

337 The protocol by Ly *et al.,* 2015 was used to extract RNA from either 50 or 100 control and *dyn-*
338 *1(RNAi)* treated gravid adult worms. One modification to the protocol involved freezing the
339 worms in the TRIzol reagent (Thermo Fisher Scientific, Catalog #15596018) at –80 °C and
340 storing them until the day of the RNA extraction. RT-PCR was performed using the Qiagen
341 OneStep RT-PCR kit (Qiagen Inc., Catalog # 210210) following the manufacturer's instructions.
342 The primers used for the RT-PCR were as follows:
343 *dyn-1* RT-PCR forward: 5'- TGTCGGAAAAGACTTCTTGC – 3'
344 *dyn-1* RT-PCR reverse: 5'- TGTCAGATTTAGAACATTTGG – 3'
345 Primers sequences targeting the *act-1* gene (loading control) were obtained from Ly *et al.* (2015).
346 act1f*:* 5'- ACGCCAACACTGTTCTTTCC – 3'
347 act1r*:* 5'- GATGATCTTGATCTTCATGGTTGA – 3'
348 Band intensities for all RT-PCR samples were quantified using the open-source software Fiji
349 (Schindelin *et al.,* 2012). Fiji was also used to convert all images to magenta and grayscale.

350 ***C. elegans* embryo live imaging using a spinning-disk confocal microscope**

351 **For imaging embryos from the IYR038 and OC779 strains depicted in Figure 1:**
352 *C. elegans* embryos obtained from dissected *smd-1(RNAi)* (control) and *dyn-1(RNAi)* worms
353 were imaged using an Olympus Yokagawa X1 spinning-disk confocal microscope as described
354 previously (Bergwell, Smith, *et al.,* 2023) with a few alterations. Timelapse imaging was
355 performed using the cellSens software (Olympus America Inc.) by taking 1.5 µm Z-stacks every
356 ~75 seconds at a 60X magnification with a 1.42 numerical aperture (NA) objective using a Prime

357 95B CMOS camera. To enable quantitative analysis, all images were captured at the same laser
358 intensity [(50% laser intensity for both 561 nm and 488 nm channels for IYR038) and (60% laser
359 intensity for 561 channel and 35% laser intensity for 488 channel for OC779)] and exposure time
360 (700 msec exposure time for both 561 nm and 488 nm channels for both strains). All brightness
361 and contrast adjustments were applied equally for both the control RNAi and *dyn-1(RNAi)*
362 representative images to enable better image presentation and viewing.

363 **For imaging embryos from the IYR038, IYR043, and IYR044 strains depicted in Figures 2-**
364 **5, Supplemental Figure S1, Supplemental Figure S2 and Supplemental Figure S3:**

365 A Nikon Ti2-E inverted microscope (Nikon Instruments Inc.) outfitted with a CREST X-Light
366 V3 spinning-disk confocal module, a motorized XY stage with encoder feedback, and a 600-µm
367 Z-piezo drive was used to make time-lapse videos of embryos. Embryos were dissected and
368 mounted on agarose pads, and coverslips were sealed with Vaseline following previously
369 described procedures (Bergwell, Smith, *et al.*, 2023). Laser illumination was supplied through a
370 Celesta solid-state light engine (Lumencor Inc.). Time-lapse image acquisition was performed in
371 NIS-Elements (Nikon Instruments Inc.), capturing 1.25-µm optical Z-stacks approximately every
372 39±4 seconds with a 60× Plan Apo λD oil-immersion objective (NA 1.42; refractive index 1.515)
373 and an ORCA-Fusion BT sCMOS detector (Hamamatsu Inc.). To ensure consistency in
374 quantitative measurements, all datasets were collected under identical exposure conditions: 200
375 msec exposure and 60% laser power at 561 nm and 400 msec exposure and 35% laser power at
376 488 nm. Maximum-intensity projections of Z-stacks were generated with NIS-Elements (Nikon
377 Instruments Inc.). For display purposes, brightness and contrast adjustments were applied
378 uniformly across the entire dataset.

379 **Spindle pole area measurement**

380 To measure spindle pole area, the cellSens software (Olympus America Inc.) was used to obtain
381 maximum intensity Z-projections of the original .vsi files. These Z-projections were saved in a
382 .png format with the fixed scaling (left:80 and right:400) for all images and further analyzed
383 using the Nikon NIS-Elements software (Nikon Instruments Inc.). The calibration on the NIS-
384 Elements software was set to 1 pixel = 0.18333 µm. The thresholding tool in NIS-Elements was
385 used to define and compute the spindle pole area (in μm^2) (intense mCherry::tubulin
386 fluorescence demarcated each spindle pole). Only regions with clearly defined spindle poles
387 were included in the analysis. Embryos in which spindle poles could not be reliably
388 distinguished were excluded. Brightness adjustments were equally applied to the images
389 representing spindle pole size in Figure 1A for better presentation and viewing.

390 **SPD-2 metaphase centrosome intensity measurements**

391 For measuring SPD-2 fluorescence intensity at centrosomes, the raw .vsi files acquired using
392 cellSens software (Olympus America Inc.) were opened in the Fiji software (Schindelin *et al.,*
393 2012) using the Bio-Formats importer plugin. The global scale was set to 1 pixel = 0.18333 µm.
394 Maximum-intensity Z-projections were generated and used for analyzing SPD-2 fluorescence
395 intensity at metaphase centrosomes. Metaphase was defined as the stage just prior to anaphase
396 onset, when the chromosomes had aligned at the cell center. A region of interest (ROI)
397 measuring 1033.33 $pixels^2$ was drawn around each metaphase centrosome and an adjacent area
398 of cytoplasm. The mean SPD-2 fluorescence intensity within each ROI (in arbitrary units, A.U.)
399 was quantified using the measure function in Fiji (Schindelin et al., 2012). Background SPD-2
400 fluorescence intensity (cytoplasmic ROI) was subtracted from the corresponding centrosomal
401 ROI value to obtain the final background-corrected SPD-2 centrosomal fluorescence intensity.
402 To calculate relative SPD-2 fluorescence levels normalized to control RNAi, all background-

403 corrected centrosomal fluorescence intensity values from both control RNAi and *dyn-1(RNAi)*
404 were divided by the mean background-corrected SPD-2 fluorescence intensity measured in
405 control RNAi embryos. Brightness, contrast, and sharpness adjustments were uniformly applied
406 to all images shown in Figure 1C to improve visualization of SPD-2 centrosome localization.
407 Embryos where the Z-projections did not capture the entire centrosome or where SPD-2 at the
408 centrosome could not be clearly identified due to surrounding debris were excluded from our
409 analysis.

410 **PLK-1 metaphase centrosome intensity measurements**

411 Metaphase was defined as the stage when the chromosomes had aligned at the center of the
412 metaphase plate. To quantify PLK-1::sfGFP fluorescence at the centrosomes, maximum intensity
413 Z-projections of metaphase embryos were generated and analyzed using Nikon NIS-Elements
414 software (Nikon Instruments Inc.). A region of interest (ROI) measuring 11.62 μm^2 was drawn
415 around each centrosome and within the cytoplasm of the same embryo. Cytoplasmic PLK-
416 1::sfGFP intensity was then subtracted from centrosomal PLK-1::sfGFP intensity to calculate the
417 background-corrected PLK-1::sfGFP centrosome fluorescence intensity, reported in arbitrary
418 units (A.U.). All background-corrected PLK-1::sfGFP centrosome intensities were divided by
419 the mean background-corrected PLK-1::sfGFP centrosome intensity of control embryos to
420 calculate the relative PLK-1 levels at centrosomes. Embryos with inaccurate PLK-1::sfGFP
421 fluorescence due to debris on top of the embryo affecting maximum intensity Z-projections or
422 instances where the Z-projections of the embryo did not cover the entire centrosome were
423 excluded from our analysis.

424 **Analysis of PLK-1 persistence at centrosomes**

425 To analyze PLK-1::sfGFP persistence at centrosomes at different cell cycle stages, maximum
426 intensity Z-projections of each timelapse sequence were quantified for centrosome-localized
427 PLK-1::sfGFP using the Nikon NIS-Elements software (Nikon Instruments Inc.). To quantify
428 centrosomal PLK-1::sfGFP levels across different cell-cycle stages, measurements were
429 restricted to the anterior centrosome. In the anterior cytoplasm, PLK-1::sfGFP background
430 fluorescence was relatively uniform, enabling consistent background subtraction and accurate
431 intensity quantification. By contrast, the posterior cytoplasm frequently exhibited irregular,
432 punctate PLK-1::sfGFP foci of variable sizes and intensities, which introduced inconsistency in
433 centrosome fluorescence measurements, especially at later cell cycle stages. For this reason,
434 posterior centrosomes were excluded from our quantitative analysis. The microtubule asters were
435 used to identify the position of the centrosomes at each cell cycle stage. A ROI of 11.62 μm^2 was
436 placed at the center of the asters as well as in its immediate vicinity (background). The PLK-
437 1::sfGFP fluorescence intensity at each anterior centrosome at every cell cycle stage was
438 determined by subtracting the background fluorescence intensity from the centrosomal
439 fluorescence intensity at that stage. Centrosomes with background-corrected PLK-1::sfGFP
440 fluorescence intensities greater than 5 arbitrary units (A.U.) were classified as "PLK-1 present"
441 whereas centrosomes with intensity values below this threshold were classified as "PLK-1
442 absent". The cell cycle stages were classified as follows: metaphase: a diamond-shaped spindle
443 formed and chromosomes aligned at the center, early anaphase: ~39±4 seconds to 78±8 seconds
444 after metaphase when the chromosomes started separating, late anaphase: ~78±8 seconds after
445 early anaphase, early telophase: ~78±8 seconds after late anaphase, and 39±4 seconds after early
446 telophase: ~39±4 seconds after early telophase. In the occasional cases where PCM disassembly
447 prevented identification of the aster center, the centrosome position from the preceding frame

448 was used as a reference. Brightness adjustments were applied equally to the representative
449 images in Figure 3A for better presentation and viewing. Only embryos where the Z-projections
450 captured the entire centrosome were used for our analysis.

451 **Quantification of midbody abnormalities**

452 Maximum-intensity Z-projections generated using Nikon NIS-Elements (Nikon Instruments Inc.)
453 were used to analyze midbody defects. Embryos were scored in a randomized and blinded
454 manner: image files were renamed with randomized identifiers and scored by an independent
455 individual. The scorer evaluated IB behavior without knowledge of genotype or treatment until
456 scoring was complete. An intercellular bridge (IB) was defined as present when a continuous,
457 tubulin-intense connection between the two daughter cells could be clearly visualized. IB
458 assembly was used as an indicator of midbody formation (Hu *et al.*, 2012; Green *et al.*, 2013;
459 König *et al.*, 2017).

460 A normal IB was defined as one that started forming approximately 195–390 seconds
461 after metaphase onset, remained stable for at least 105 seconds following its formation, and
462 exhibited the stereotypical IB assembly dynamics. Stereotypical IB dynamics consisted of a
463 sequence in which the spindle midzone coalesced into a single focused, microtubule-rich bridge-
464 like IB structure. Following coalescence, the IB typically increased in tubulin intensity, then
465 gradually decreased in intensity as it regressed. Once coalesced, normal IBs did not separate or
466 fragment and maintained a continuous tubulin-dense morphology until midbody resolution.

467 An abnormal IB was defined as one that failed to exhibit this stereotypical progression.
468 Abnormal IBs included bridges that did not start forming within the 195–390 second window,
469 did not coalesce into a single focused structure, showed fluctuating tubulin intensity, or came
470 apart after coalescence. An embryo was scored as lacking an IB when no stable IB could be

471 detected at any point during the remainder of the cell cycle and through the onset of centrosome
472 separation in the next cell cycle.
473 Embryos where the entire IB was not captured in the maximum intensity Z-projections
474 were excluded from our analysis. For better visualization and presentation, brightness and
475 contrast setting were applied uniformly and equally to all the representative images in Figure 4A.
476 **Quantification of PLK-1 localization at the midbody**
477 PLK-1 localization at the midbody was quantified using a blinded, randomized analysis using
478 maximum intensity Z-projections that were generated with the Nikon NIS-Elements software
479 (Nikon Instruments Inc.). All image files were renamed with random alphanumeric identifiers by
480 an independent individual who was not involved in the scoring. The scorer analyzed the
481 randomized dataset without knowledge of genotype, treatment condition, or imaging sequence.
482 After all scoring was completed and recorded, the mapping key was revealed to assign quantified
483 values back to experimental groups.
484 An IB/midbody was defined as present when a continuous, tubulin-intense connection
485 between the two daughter cells could be clearly visualized in Z-projections. An IB was
486 considered to have formed if it remained cohesive for at least ~105 seconds after its appearance.
487 Metaphase was defined as the timepoint immediately after nuclear envelope breakdown when the
488 chromosomes are aligned centrally at the metaphase plate. For event-matched analysis, a normal
489 PLK-1 localization pattern was defined as a continuous, dot-like or band-like PLK-1::sfGFP
490 signal above the local background at the IB center. Abnormal localization was defined as
491 discontinuous, fragmented, or off-center PLK-1::sfGFP fluorescence, or a reduced signal that
492 was either at or below the local background. For the time-matched analysis, cases where PLK-
493 1::sfGFP localized to the IB were scored as “localized” and those where it failed to localize to

494 the IB either because IB formation was delayed or because an IB did not form were scored as
495 "did not localize". For all analyses, PLK-1 localization was scored at the frame in which the IB
496 was fully formed, and just before the tubulin intensity at the IB began to decrease, ensuring that
497 measurements were taken while the midbody remained structurally relatively intact.

498 For time-matched analysis, PLK-1::sfGFP fluorescence was assessed relative to the
499 reference window during which stable IB formation normally begins in control embryos (195–
500 390 seconds after metaphase onset).

501 For event-matched analysis, PLK-1::sfGFP fluorescence was assessed whenever a stable
502 IB formed, even if the IB formed outside of the normal developmental window for bridge
503 assembly.

504 Z-projections in which either the IB or midbody-associated PLK-1 were not fully
505 captured across the Z-stack were excluded from analysis to ensure accurate evaluation of PLK-1
506 fluorescence at the IB/midbody. Brightness adjustments were applied equally to all merged and
507 all PLK-1::sfGFP representative images of PLK-1 midbody localization in Figure 5A.

508 **Embryo size measurements**

509 Nikon-NIS Elements (Nikon Instruments Inc.) was used to generate maximum intensity Z-
510 projections of the raw data and to measure the sizes of metaphase-stage 1-cell *C. elegans*
511 embryos. To measure embryo size, the Bézier tool in NIS-Elements was used to manually trace
512 the outline of each embryo, using cytoplasmic PLK-1::sfGFP fluorescence to define the
513 cytoplasmic embryo boundary. The enclosed area was calculated by the software and reported in
514 μm^2. Embryos whose boundaries could not be clearly defined by cytoplasmic PLK-1::sfGFP
515 fluorescence due to embryo orientation were excluded from the analysis.

516 **Cytoplasmic PLK-1 fluorescence measurements**

517 Maximum intensity Z-projections generated by Nikon NIS-Elements (Nikon Instruments Inc.)
518 were used to measure cytoplasmic PLK-1::sfGFP in the anterior and posterior cytoplasm of wild-
519 type and *dyn-1(ky51)* embryos. For these measurements, the Z-projections were opened in NIS-
520 Elements and a large ROI of 128.97 μm^2 was placed within the anterior and posterior cytoplasm
521 of metaphase-stage embryos away from the spindle apparatus. The mean PLK-1::sfGFP
522 fluorescence intensities within these ROIs were determined using the NIS-Elements software and
523 reported in arbitrary units (A.U.). Measurements in which the ROI could not fit within the
524 embryo boundaries due to smaller embryo size were excluded from our analysis.

525 **Statistical analysis**

526 Graphpad prism 10.5 and 10.6.1 (GraphPad Software, Inc., San Diego, CA) were used to
527 perform statistical analyses of all the data. For all the data, error bars represent the standard
528 deviation (s.d.) above and below the mean and the middle lines represent the mean. p-values
529 were rounded to two decimal places and considered significant if $p<0.05$. A two-tailed unpaired
530 t-test was used to analyze: spindle pole area (Figure 1B), SPD-2 fluorescence intensity (Figure
531 1D), PLK-1::sfGFP centrosome fluorescence intensities at different cell cycle stages
532 (Supplemental Figure S3), *dyn-1* knockdown by RT-PCR (Supplemental Figure S1B), embryo
533 size (cytoplasmic area) (Supplemental Figure S1D), and cytoplasmic PLK-sfGFP intensity
534 (Supplemental Figure S2). A Fisher's exact test was used to analyze the PLK-1::sfGFP
535 persistence at the centrosomes (Figure 3B), and defects in PLK-1::sfGFP localization to the
536 midbody (Figure 5, B and C).

537 **ACKNOWLEDGMENTS**

538 This work was supported by NIH/NIGMS grants (5P20GM103636-09 and 7R15GM152965-02)
539 and start-up funding from North Carolina A&T State University to J.I. Additional support was

540 provided by NIH/NIGMS grant 1R35GM153737 and NCI grant 1R01CA273095 to R.N. We
541 would like to acknowledge Dr. Hailey Edigo-Betancourt, Jasmyn Grant, Journey Reddick-
542 Umoja, Erin Haastrup, Peter Nunan, and Mariah Moreland for technical assistance. OC908 and
543 OC779 strains were provided by Dr. Kevin O'Connell (NIDDK, NIH). Some strains used in this
544 study were provided by the CGC, which is funded by NIH Office of Research Infrastructure
545 Programs (P40 OD010440). The authors declare no competing interests.

546 **REFERENCES**

547 Archambault V, Glover DM (2009). Polo-like kinases: conservation and divergence in their
548 functions and regulation. **Nat Rev Mol Cell Biol** *10*, 265–275.
549 Arnaud L, Pines J, Nigg EA (1998). GFP tagging reveals human Polo-like kinase 1 at the
550 kinetochore/centromere region of mitotic chromosomes. **Chromosoma** *107*, 424–429.
551 Barr FA, Silljé HHW, Nigg EA (2004). Polo-like kinases and the orchestration of cell division.
552 **Nat Rev Mol Cell Biol** *5*, 429–441.
553 Bergwell M, Smith A, Smith E, Dierlam C, Duran R, Haastrup E, Napier-Jameson R, Seidel R,
554 Potter W, Norris A, et al. (2023). A primary microcephaly-associated *sas-6* mutation perturbs
555 centrosome duplication, dendrite morphogenesis, and ciliogenesis in *Caenorhabditis elegans*.
556 **Genetics** *224*, iyad105.
557 Boxem M, Maliga Z, Klitgord N, Li N, Lemmens I, Mana M, De Lichtervelde L, Mul JD, Van
558 De Peut D, Devos M, et al. (2008). A protein domain-based interactome network for *C. elegans*
559 early embryogenesis. **Cell** *134*, 534–545.
560 Budirahardja Y, Gönczy P (2008). PLK-1 asymmetry contributes to asynchronous cell division
561 of *Caenorhabditis elegans* embryos. **Development** *135*, 1303–1313.

562 Chase D, Serafinas C, Ashcroft N, Kosinski M, Longo D, Ferris DK, Golden A (2000). The
563 polo-like kinase PLK-1 is required for nuclear envelope breakdown and the completion of
564 meiosis in *Caenorhabditis elegans*. **Genesis** *26*, 26–41.
565 Chen YZ, Zimyanin V, Redemann S (2023). Loss of the mitochondrial protein SPD-3 elevates
566 PLK-1 levels and dysregulates mitotic events. **Life Sci Alliance** *6*, e202302117.
567 Clark SG, Shurland DL, Meyerowitz EM, Bargmann CI, Van der Bliek AM (1997). A dynamin
568 GTPase mutation causes a rapid and reversible temperature-inducible locomotion defect in
569 *Caenorhabditis elegans*. **Proc Natl Acad Sci USA** *94*, 10438–10443.
570 Decker M, Jaensch S, Pozniakovsky A, Zinke A, O'Connell KF, Zachariae W, Myers E, and
571 Hyman AA (2011). Limiting amounts of centrosome material set centrosome size in *C. elegans*
572 embryos. **Curr Biol** *21*, 1259–1267.
573 Golsteyn RM, Mundt KE, Fry AM, Nigg EA (1995). Cell cycle regulation of the activity and
574 subcellular localization of Plk1, a human protein kinase implicated in mitotic spindle function. **J**
575 **Cell Biol** *129*, 1617–1628.
576 Gomez-Ferreria MA, Rath U, Buster DW, Chanda SK, Caldwell JS, Rines DR, Sharp DJ (2007).
577 Human Cep192 is required for mitotic centrosome and spindle assembly. **Curr Biol** *17*, 1960–
578 1966.
579 Grant B, Hirsh D (1999). Receptor-mediated endocytosis in the *Caenorhabditis elegans* oocyte.
580 **Mol Biol Cell** *10*, 4311–4326.
581 Green, R.A., J.R. Mayers, S. Wang, L. Lewellyn, A. Desai, A. Audhya, and K. Oegema (2013).
582 The midbody ring scaffolds the abscission machinery in the absence of midbody microtubules. **J**
583 **Cell Biol.** *203*, 505–520.

584 Hinshaw JE (2000). Dynamin and its role in membrane fission. **Annu Rev Cell Dev Biol** *16*,
585 483–519.
586 Hu CK, Coughlin M, Mitchison TJ (2012). Midbody assembly and its regulation during
587 cytokinesis. **Mol Biol Cell** *23*, 1024–1034.
588 Iyer J, Gentry LK, Bergwell M, Smith A, Guagliardo S, Kropp PA, Sankaralingam P, Liu Y,
589 Spooner E, Bowerman B, et al. (2022). The chromatin remodeling protein CHD-1 and the EFL-
590 1/DPL-1 transcription factor cooperatively downregulate CDK-2 to control SAS-6 levels and
591 centriole number. **PLoS Genet** *18*, e1009799.
592 Iyer J, DeVaul N, Hansen T, Nebenfuehr B (2019). Using microinjection to generate genetically
593 modified *Caenorhabditis elegans* by CRISPR/Cas9 editing. In: *Microinjection: Methods and*
594 *Protocols*, ed. C Liu and Y Du, New York, NY: Humana Press, 431–457.
595 Kamath RS, Ahringer J (2003). Genome-wide RNAi screening in *Caenorhabditis elegans*.
596 **Methods** *30*, 313–321.
597 Kemp CA, Kopish KR, Zipperlen P, Ahringer J, O'Connell KF (2004). Centrosome maturation
598 and duplication in *C. elegans* require the coiled-coil protein SPD-2. **Dev Cell** *6*, 511–523.
599 Kishi K, Van Vugt MA, Okamoto KI, Hayashi Y, Yaffe MB (2009). Functional dynamics of
600 Polo-like kinase 1 at the centrosome. **Mol Cell Biol** *29*, 3134–3150.
601 König J, Frankel EB, Audhya A, Müller-Reichert T (2017). Membrane remodeling during
602 embryonic abscission in *Caenorhabditis elegans*. **J Cell Biol** *216*, 1277–1286.
603 Lee KS, Yuan YL, Kuriyama R, Erikson RL (1995). Plk is an M-phase-specific protein kinase
604 and interacts with a kinesin-like protein, CHO1/MKLP1. **Mol Cell Biol** *15*, 7143–7151.
605 Levine MS, Holland AJ (2018). Impact of mitotic errors on cell proliferation and tumorigenesis.
606 **Genes Dev** *32*, 620–638.

607 Ly K, Reid SJ, Snell RG (2015). Rapid RNA analysis of individual *Caenorhabditis elegans*.
608 **MethodsX** *2*, 59–63.
609 Martino L, Morchoisne Bolhy S, Cheerambathur DK, Van Hove L, Dumont J, Joly N, Desai A,
610 Doye V, Pintard L (2017). Channel nucleoporins recruit PLK-1 to nuclear pore complexes to
611 direct nuclear envelope breakdown in *C. elegans*. **Dev Cell** *43*, 157–171.
612 O'Connell KF, Maxwell KN, White JG (2000). The *spd-2* gene is required for axis polarization
613 in the *C. elegans* zygote. **Dev Biol** *222*, 55–70.
614 Paix A, Folkmann A, Rasoloson D, Seydoux G (2015). High efficiency, homology-directed
615 genome editing in Caenorhabditis elegans using CRISPR-Cas9 ribonucleoprotein complexes.
616 **Genetics** *201*, 47–54.
617 Paix A, Schmidt H, Seydoux G (2016). Cas9-assisted recombineering in *C. elegans*: genome
618 editing using in vivo assembly of linear DNAs. **Nucleic Acids Res** *44*, e128.
619 Paschal BM, Shpetner HS, Vallee RB (1987). MAP 1C is a microtubule-activated ATPase which
620 translocates microtubules in vitro and has dynein-like properties. **J Cell Biol** *105*, 1273–1282.
621 Pelletier L, Özlü N, Hannak E, Cowan C, Habermann B, Ruer M, Müller-Reichert T, Hyman AA
622 (2004). The *Caenorhabditis elegans* centrosomal protein SPD-2 is required for both
623 pericentriolar material recruitment and centriole duplication. **Curr Biol** *14*, 863–873.
624 Petronczki M, Lénárt P, Peters JM (2008). Polo on the rise—from mitotic entry to cytokinesis
625 with Plk1. **Dev Cell** *14*, 646–659.
626 Praefcke GJA, McMahon HT (2004). The dynamin superfamily: universal membrane tubulation
627 and fission molecules?. **Nat Rev Mol Cell Biol** *5*, 133–147.

628 Schindelin J, Arganda-Carreras I, Frise E, Kaynig V, Longair M, Pietzsch T, Preibisch S,
629 Rueden C, Saalfeld S, Schmid B, Tinevez J-Y, et al. (2012). Fiji: an open-source platform for
630 biological-image analysis. **Nat Methods** *9*, 676–682.
631 Schmucker S, Sumara I (2014). Molecular dynamics of PLK1 during mitosis. **Mol Cell Oncol** 1,
632 e954507.
633 Shpetner HS, Vallee RB (1989). Identification of dynamin, a novel mechanochemical enzyme
634 that mediates interactions between microtubules. **Cell** *59*, 421–432.
635 Smith A, Bergwell M, Smith E, Mathew D, Iyer J (2020). CRISPR/Cas9 editing of the *C.*
636 *elegans rbm-3.2* gene using the *dpy-10* Co-CRISPR screening marker and assembled
637 ribonucleoprotein complexes. **J Vis Exp** *166*, e62001.
638 Sugioka K, Hamill DR, Lowry JB, McNeely ME, Enrick M, Richter AC, Kiebler LE, Priess JR,
639 Bowerman B (2017). Centriolar SAS-7 acts upstream of SPD-2 to regulate centriole assembly
640 and pericentriolar material formation. **eLife** *6*, e20353.
641 Thompson HM, Skop AR, Euteneuer U, Meyer BJ, McNiven MA (2002). The large GTPase
642 dynamin associates with the spindle midzone and is required for cytokinesis. **Curr Biol** *12*,
643 2111–2117.
644 Zhu F, Lawo S, Bird A, Pinchev D, Ralph A, Richter C, Müller-Reichert T, Kittler R, Hyman
645 AA, Pelletier L (2008). The mammalian SPD-2 ortholog Cep192 regulates centrosome
646 biogenesis. **Curr Biol** *18*, 136–141.
647 Zitouni S, Nabais C, Jana SC, Guerrero A, Bettencourt-Dias M (2014). Polo-like kinases:
648 structural variations lead to multiple functions. **Nat Rev Mol Cell Biol** *15*, 433–452.

649 **FIGURE LEGENDS**

650 FIGURE 1. DYN-1 depletion increases spindle pole size and elevates SPD-2 at centrosomes. (A)
651 Spindle pole morphology in embryos expressing mCherry::tubulin, showing enlarged spindle
652 poles upon *dyn-1(RNAi)*. White arrows: spindle poles. (B) Quantification of spindle pole area
653 using mCherry::tubulin fluorescence. Each point = single pole; n = spindle poles analyzed. Error
654 bars = s.d.; middle bar = mean. (C) SPD-2 localization at metaphase centrosomes in control and
655 *dyn-1(RNAi)* embryos. Dotted outline demarcates the embryo boundary; white arrows:
656 centrosome-localized SPD-2 (D) Relative centrosomal SPD-2 intensity normalized to control
657 RNAi. n = centrosomes. Error bars = s.d.; middle bar = mean. (B, D): unpaired two-tailed t-test;
658 Experimental replicates: 4 for all assays. All fluorescence images include a 10 µm scale bar.
659
660 FIGURE 2. DYN-1 depletion increases centrosomal PLK-1 at metaphase. (A) PLK-1::sfGFP
661 localization at metaphase centrosomes in control RNAi vs *dyn-1(RNAi)* embryos. White arrows:
662 centrosome-localized PLK-1::sfGFP. (B) Quantification of PLK-1::sfGFP centrosomal
663 fluorescence at metaphase. n = centrosomes. Error bars = s.d.; middle bar = mean. (C) PLK-
664 1::sfGFP localization in wild-type (wt) *dyn-1* and *dyn-1(ky51)*. White arrows: centrosome-
665 localized PLK-1::sfGFP. (D) Relative centrosomal PLK-1 intensity in wild-type (wt) *dyn-1* and
666 *dyn-1(ky51)*. n = centrosomes. Error bars = s.d.; middle bar = mean. (B, D): unpaired two-tailed
667 t-test; Experimental replicates: 3 for all assays. All fluorescence images include a 10 µm scale
668 bar.
669
670 FIGURE 3. PLK-1 persists abnormally at centrosomes during mitotic progression in *dyn-*
671 *1(RNAi)* embryos. (A) Time-lapse analysis of different mitotic stages in control RNAi and *dyn-*
672 *1(RNAi)* embryos. White arrows: anterior centrosome-localized PLK-1::sfGFP. (B) Percentage

673 of centrosomes retaining PLK-1 at each stage. Fisher's Exact Test; ns= not significant; n =
674 centrosomes analyzed. Experimental replicates: 3 for all assays. All fluorescence images include
675 a 10 µm scale bar.
676
677 FIGURE 4. DYN-1 depletion disrupts Intercellular Bridge (IB) assembly. (A) Time-lapse images
678 of mCherry::tubulin showing normal IB formation in control RNAi embryos (top panel) and
679 abnormal (middle panel) or missing (bottom panel) IBs in *dyn-1(RNAi)* embryos. White arrows:
680 IB (B) Classification of IB morphology (normal, abnormal, absent). n = embryos analyzed.
681 Experimental replicates: 3 for all assays. All fluorescence images include a 10 µm scale bar.
682
683 FIGURE 5. PLK-1 localization at the midbody is defective in *dyn-1(RNAi)* embryos. (A) Time-
684 matched and event-matched PLK-1::sfGFP localization at the midbody in control RNAi and *dyn-*
685 *1(RNAi)* embryos. White arrows: IB; yellow arrows: PLK-1::sfGFP at IB (B) Time-matched
686 PLK-1 scoring at the midbody. n = embryos; Fisher's Exact Test. (C) Event-matched PLK-1
687 scoring at the midbody. n = embryos; Fisher's Exact Test. Experimental replicates: 3 for all
688 assays. All fluorescence images include a 10 µm scale bar.
689 **SUPPLEMENTAL FIGURES**
690 FIGURE S1. *dyn-1(RNAi)* reduces *dyn-1* mRNA levels and decreases embryo size. (A) RT-PCR
691 validation of *dyn-1* depletion. (B) Relative *dyn-1* mRNA quantification. Error bars = s.d. (C)
692 Comparison of average embryo sizes in control RNAi and *dyn-1(RNAi)*. (D) Cytoplasmic area
693 quantification using PLK-1::sfGFP fluorescence as a marker for the cytoplasmic embryo border.
694 n = embryos. Error bars = s.d.; middle bar = mean. (B, D): unpaired two-tailed t-test;
695 Experimental replicates: 3 for all assays. All fluorescence images include a 10 µm scale bar.

696

697 FIGURE S2. Cytoplasmic PLK-1::sfGFP levels are modestly elevated in *dyn-1(ky51)* embryos as
698 compared to wild-type. (A) Quantification of anterior and posterior cytoplasmic PLK-1::sfGFP
699 in wild-type (wt) *dyn-1* and *dyn-1(ky51)* embryos. A.U.= Arbitrary Units; unpaired two-tailed t-
700 test; n = measurements. Error bars = s.d.; middle bar = mean. Experimental replicates: 3.

701

702 FIGURE S3. Comparison of centrosomal PLK-1 intensity across cell cycle stages in control
703 RNAi and *dyn-1(RNAi)* embryos. (A) Centrosomal PLK-1::sfGFP intensity at metaphase, early
704 and late anaphase, early telophase, and 39±4 seconds post early telophase. A.U.= Arbitrary
705 Units; unpaired two-tailed t-test; n = 29 centrosomes (control RNAi); n = 26 centrosomes (*dyn-*
706 *1(RNAi))*. Error bars = s.d.; middle bar = mean. Experimental replicates: 3.

707

Figure 1

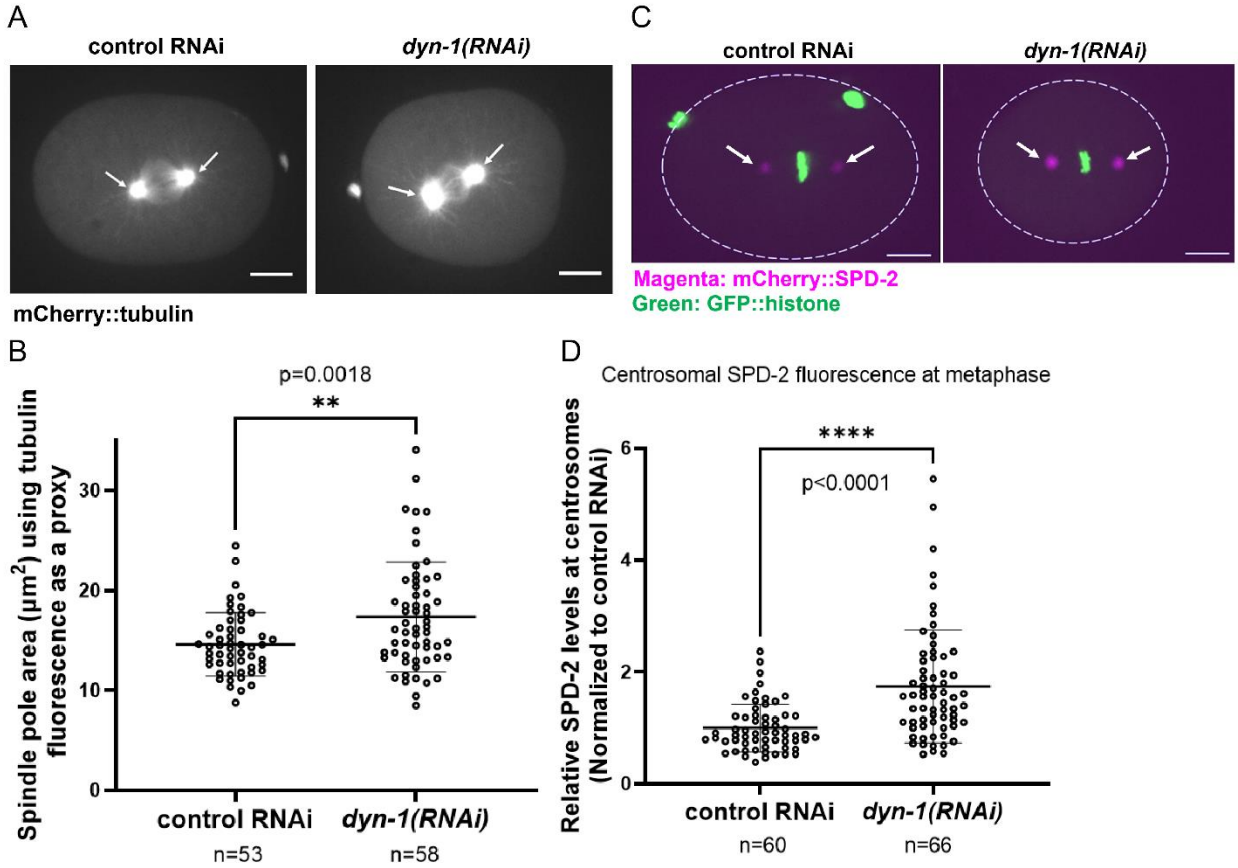
A
control RNAi
dyn-1(RNAi)
mCherry::tubulin
C
control RNAi
dyn-1(RNAi)
Magenta: mCherry::SPD-2
Green: GFP::histone
B
p=0.0018
**
Spindle pole area (µm²) using tubulin fluorescence as a proxy
0
10
20
30
control RNAi
dyn-1(RNAi)
n=53
n=58
D
Centrosomal SPD-2 fluorescence at metaphase
****
p<0.0001
Relative SPD-2 levels at centrosomes (Normalized to control RNAi)
0
2
4
6
control RNAi
dyn-1(RNAi)
n=60
n=66

Figure 2

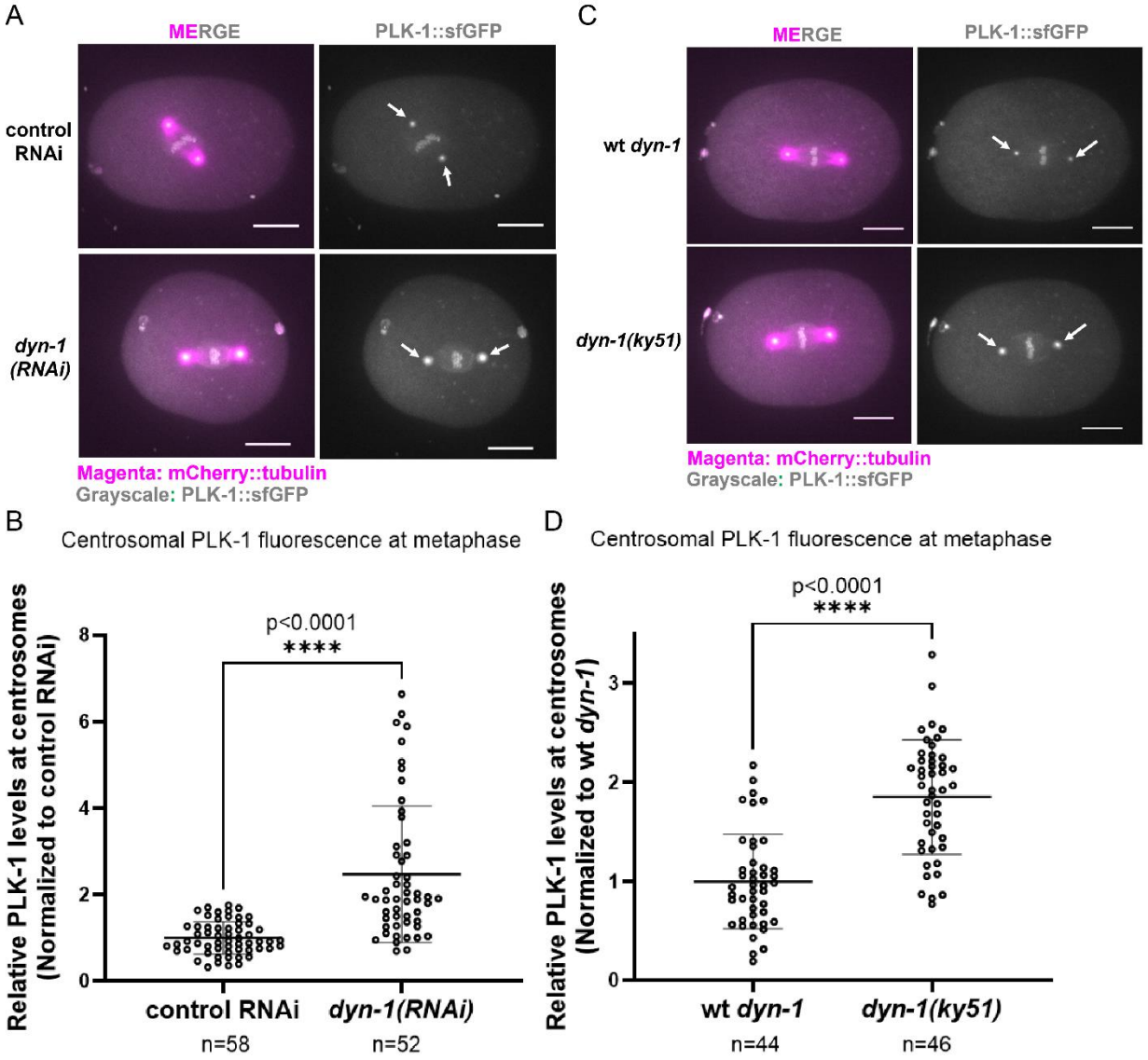
A
MERGE
PLK-1::sfGFP
control RNAi
dyn-1 (RNAi)
Magenta: mCherry::tubulin
Grayscale: PLK-1::sfGFP
C
MERGE
PLK-1::sfGFP
wt dyn-1
dyn-1(ky51)
Magenta: mCherry::tubulin
Grayscale: PLK-1::sfGFP
B
Centrosomal PLK-1 fluorescence at metaphase
Relative PLK-1 levels at centrosomes (Normalized to control RNAi)
p<0.0001
****
control RNAi
dyn-1(RNAi)
n=58
n=52
D
Centrosomal PLK-1 fluorescence at metaphase
Relative PLK-1 levels at centrosomes (Normalized to wt dyn-1)
p<0.0001
****
wt dyn-1
dyn-1(ky51)
n=44
n=46

Figure 3

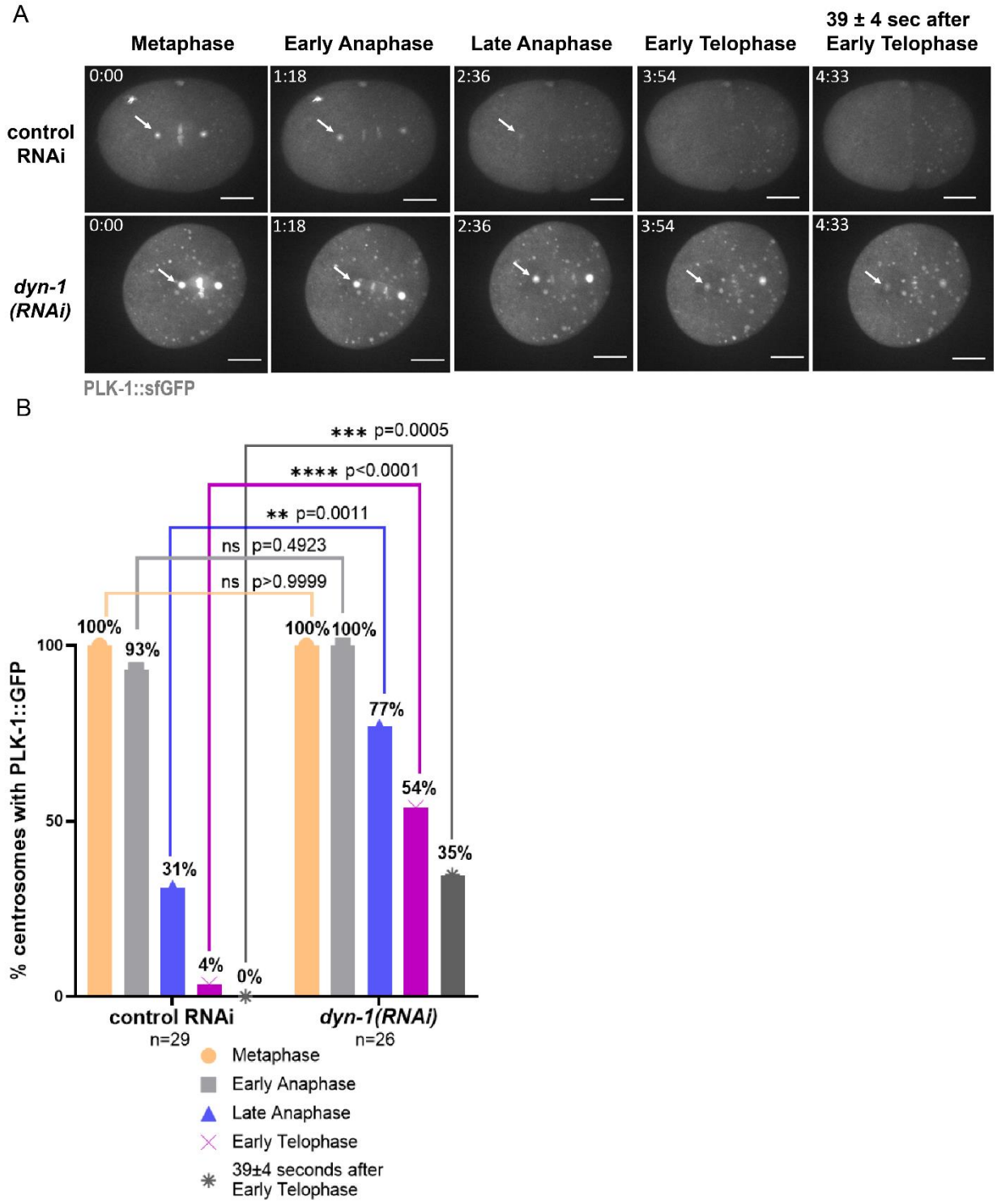
A
Metaphase
Early Anaphase
Late Anaphase
Early Telophase
39 ± 4 sec after Early Telophase
control RNAi
dyn-1 (RNAi)
0:00
1:18
2:36
3:54
4:33
PLK-1::sfGFP
B
*** p=0.0005
**** p<0.0001
** p=0.0011
ns p=0.4923
ns p>0.9999
% centrosomes with PLK-1::GFP
100
50
0
100%
93%
31%
4%
0%
100%
100%
77%
54%
35%
control RNAi
n=29
dyn-1(RNAi)
n=26
Metaphase
Early Anaphase
Late Anaphase
Early Telophase
39±4 seconds after Early Telophase

Figure 4

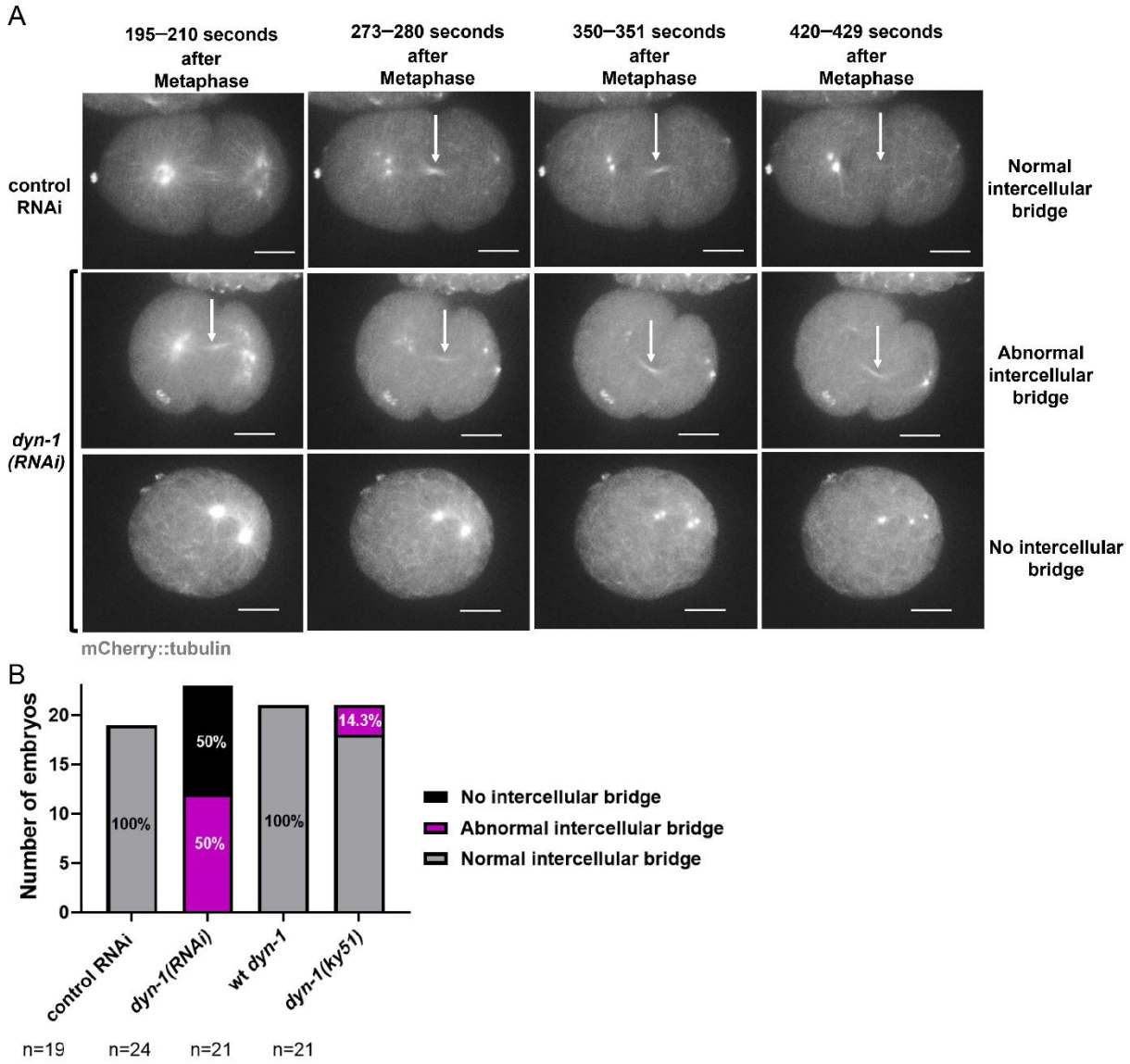
A
195–210 seconds after Metaphase
273–280 seconds after Metaphase
350–351 seconds after Metaphase
420–429 seconds after Metaphase
control RNAi
dyn-1 (RNAi)
Normal intercellular bridge
Abnormal intercellular bridge
No intercellular bridge
mCherry::tubulin
B
Number of embryos
20
15
10
5
0
100%
50%
50%
100%
14.3%
No intercellular bridge
Abnormal intercellular bridge
Normal intercellular bridge
control RNAi
dyn-1(RNAi)
wt dyn-1
dyn-1(ky51)
n=19
n=24
n=21
n=21

Figure 5

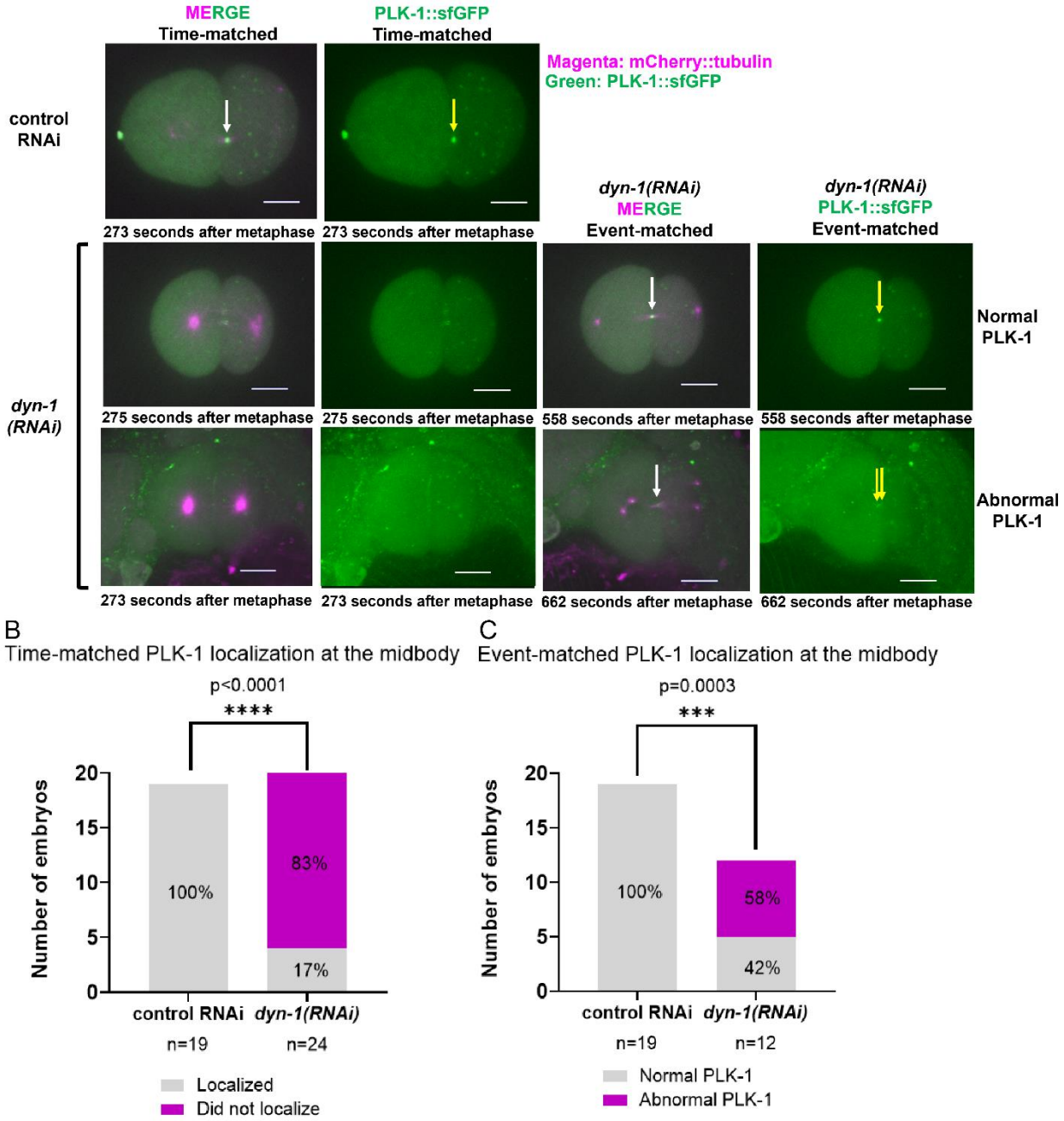
MERGE
Time-matched
PLK-1::sfGFP
Time-matched
Magenta: mCherry::tubulin
Green: PLK-1::sfGFP
control RNAi
273 seconds after metaphase
273 seconds after metaphase
dyn-1(RNAi)
MERGE
Event-matched
dyn-1(RNAi)
PLK-1::sfGFP
Event-matched
dyn-1 (RNAi)
275 seconds after metaphase
275 seconds after metaphase
558 seconds after metaphase
558 seconds after metaphase
Normal PLK-1
Abnormal PLK-1
273 seconds after metaphase
273 seconds after metaphase
662 seconds after metaphase
662 seconds after metaphase
B
Time-matched PLK-1 localization at the midbody
p<0.0001
****
Number of embryos
20
15
10
5
0
100%
83%
17%
control RNAi
dyn-1(RNAi)
n=19
n=24
Localized
Did not localize
C
Event-matched PLK-1 localization at the midbody
p=0.0003
***
Number of embryos
20
15
10
5
0
100%
58%
42%
control RNAi
dyn-1(RNAi)
n=19
n=12
Normal PLK-1
Abnormal PLK-1